J Solid State Electrochem (2009) 13:687–695
DOI 10.1007/s10008-008-0565-8

ORIGINAL PAPER

Electrochromic responses of low-temperature-annealed tungsten oxide thin films in contact with a liquid and a polymeric gel electrolyte

L. Hechavarría · H. Hu · M. Miranda · M. E. Nicho

Received: 10 December 2007 / Accepted: 17 April 2008 / Published online: 17 June 2008

Abstract Thin films of tungsten trioxide (WO_3) for electrochromic application were synthesized by potentiostatic method by using a peroxytungstic acid as a solution precursor. The morphology of the films with and without postthermal annealing was analyzed by atomic force microscopy. When they were in contact with the liquid electrolyte (LiI in propylene carbonate, PC) and under alternatively applied negative (−1.5 V) and positive (+1.0 V) potentials, the transient optical transmittance modulations at wavelength of 650 nm of the as-deposited and 60 °C annealed WO_3 samples were higher than that of 100 °C annealed WO_3 films, and the switching times between the colored and bleached states were related to the surface morphology of the WO_3 films. In polymeric gel electrolyte (LiI and polymethyl methacrylate in PC) devices, longer time was required for complete coloration as well as bleaching process compared with the liquid one. A parametric analysis was made for each of the transient optical transmittance curves of WO_3-based electrochromic devices to extract the values of the response time in coloration (reduction) and bleaching (oxidation) processes. It concludes that the coloration process was determined by the exchange of current density at the electrolyte–WO_3 interface and a possible inhomogeneous interfacial potential for ion intercalation retards the effective coloration time. The bleaching process seems to be controlled by the space charge-limited lithium ion diffusion in WO_3 electrode and the ionic conductivity of the electrolyte as well.

Keywords Electrochromic properties · Surface morphology · WO_3 thin films · Polymeric gel electrolyte · Transient optical responses

L. Hechavarría · H. Hu (✉) · M. Miranda
Centro de Investigación en Energía,
Universidad Nacional Autónoma de México,
Priv. Xochicalco S/N,
Temixco 62580 Morelos, México
e-mail: hzh@cie.unam.mx

M. E. Nicho
Centro de Investigación en Ingeniería
y Ciencias Aplicadas, UAEM,
Av. Universidad 1001, Col. Chamilpa,
C.P. 62210 Cuernavaca, Morelos, México

Introduction

The development of efficient electrochromic devices (ECDs) has received considerable attention during the last 25 years because of their potentiality of being used for energy saving and human comfort in buildings. Tungsten trioxide, WO_3, is the most studied electrochromic material due to its promising dynamic controller of solar energy [1–2]. It can be prepared by sol-gel process [3–7], magnetron sputtering [8–10], thermal evaporation [11–12], and cathodic electrodeposition [13–17]. The last one is a widely used and simple technique for WO_3 thin film preparation.

On the other hand, the idea of using solar energy to switch an ECD leads to the attempt to integrate an ECD with a photovoltaic cell to form the so-called photoelectrochromic device. It consists in a photovoltaic electrode, an electrochromic-material-coated counter electrode, and an electrolyte in between that balances the charge transfer inside the cell through a redox pair (I^-/I^{3-}, for example). The color change of the electrochromic electrode is caused by the photovoltage generated from the illuminated photovoltaic electrode. Namely, the energy required for color switch comes from solar radiation, saving in this way the external electrical energy supply for ECD. The first photoelectrochromic cell was reported in 1997 that contained a dye-sensitized TiO_2 electrode, a WO_3-thin-film-

coated electrochromic electrode and a liquid electrolyte containing I^-–I^{3-} [18]. One of the attractive aspects in this design is the possibility of the independent optimization in each of the two electrodes of the system. But its disadvantage is the poor durability, especially at high temperatures [19–23], due to the solvent loss caused by its volatile nature, decomposition, and contamination with water and impurities. Therefore, substitution of liquid electrolytes has received increasing attention for application purpose, and the research works have been addressed to the use of solid or viscous electrolytes to overcome the instability problem in the above-mentioned devices.

The objective of this paper is to compare the electrochromic properties of electrochemically deposited WO_3 thin films in contact with a gel polymer electrolyte and with a liquid one. All devices were prepared in sandwich or laminated structure. The effect of low-temperature annealing of the WO_3 films on their electrochromic performance is also analyzed.

Experimental

Synthesis of precursor sol and film deposition

Peroxytungstic acid was prepared by dissolving 1 g of tungsten (Spectrum) in 10 mL of hydrogen peroxide (30%, Fermont). After the metal was completely dissolved and the exothermic reaction was over, platinum sheet was introduced into solution to reduce the excess of peroxide. The solution was diluted to 0.05 mol/L with 70/30 *v*/*v* deionized water–2-propanol to improve the solution stability and stored in dark.

The predominant peroxytungstate in the acidic solution is reported to be $(W_2O_{11})^{2-}$, or $[((O)W(O_2))_2(O)(O_2)_2W(O)]^{2-}$, where (O_2) denotes a peroxide ligand. Seven coordinations are completed by hydration [14]. The anion is formed according to:

$$2W + 10H_2O_2 \rightarrow (W_2O_{11})^{2-} + 2H^+ + 9H_2O$$

WO_3 films were obtained at room temperature by cathodic electrodeposition in a three-electrode electrochemical cell with a platinum sheet as the auxiliary electrode, an indium tin oxide (ITO)-coated glass sheet (8–12 Ω per square, Delta Technologies) as the working electrode, and standard calomel electrode as reference. The working electrode was subjected to a constant cathodic potential of −0.5 V and the total deposition time was about 10 min. After withdrawing from the solution, the films were rinsed with deionized water and dried in air. In order to determine the density of injected charge or ion storage capacity, WO_3 films were taken out of the solution when they were totally oxidized (transparent). Some of the as-deposited WO_3 films were annealed at 60 °C for 2 h or at 100 °C for 1 h.

Preparation of electrolytes and devices

Two types of electrolytes were used for assembling electrochromic cells: the liquid one, composed of 0.5 mol/L lithium iodide (LiI) in propylene carbonate (PC), and a quasisolid or viscous one, prepared by dissolving 0.7g of polymethyl methacrylate (PMMA; MW=120,000) and 0.53 g of LiI in 3.3 mL of PC. The devices were assembled by applying the electrolyte between WO_3 and an ITO glass and sealed with silicone. The effective area of the devices was about 1 cm^2. At room temperature, the conductivity of the gel polymer electrolyte was 2.27×10^{-5} Ω^{-1} cm^{-1}, and at 70 °C, 3.1×10^{-5} Ω^{-1} cm^{-1}, measured by electrochemical impedance spectroscopy (VoltaLab PGZ301, Dynamic-EIS).

Material and device characterization

The average thickness of WO_3 films was about 250 nm, measured by a perfilometer Alpha Step (100 Tencor instruments). Crystalline structure of WO_3 films was analyzed by X-ray diffraction (XRD, Cu kα Rigaku DMAX-2200 X-ray diffractometer) at a low incident angle (0.5°) to diminish the ITO phase signal in the XRD spectra. The surface morphology of WO_3 films was analyzed by atomic force microscopy (AFM, Autoprobe CP, Park Scientific Microscopy). The electrochemical characterization of the WO_3-based devices with liquid or polymeric gel electrolyte was realized by cyclic voltammetry. No reference electrode was used for all the electrochemical measurements in this work. The Li^+ ion diffusion coefficient in WO_3 films was studied by chronopotentiometric method by applying a current pulse of 100 μA for 20 s. The ion storage capability, or charge injected in WO_3 films, was determined by a chronoamperometric method applying a potential pulse of −1.5 V for 20 s. Cyclic voltammetry, chronoamperometry, and chronopotentiometry were realized in a SOLARTRON: SI1287, electrochemical interface. Optical transmission modulation or transient optical transmittance curves (ΔT, %) as well as optical transmittance spectra of WO_3 films and devices were recorded on an UV-VIS spectrophotometer (Shimadzu 3101 PC). A homemade voltage source was used to apply a direct current potential to the WO_3-based electrochromic devices.

Results and discussion

WO_3 films

During the electrodeposition of WO_3, the color of the deposited films changed gradually from clear blue at about 3 min to dark blue at 10 min of deposition time. It suggests that a nonstoichiometric tungsten oxide was formed at a

cathodic potential. However, with exposure in ambient atmosphere for about 20 h, the blue films turn to be bleached. Optical absorbance and transmittance spectra of a freshly deposited WO_3 film and 1-day-after-deposition (as-deposited) WO_3 sample were shown in Fig. 1. It is observed that the oxidation of the freshly WO_3 sample in air (with a humidity of about 35%) reduces its absorbance (and possibly reflectance) in visible and near-infrared region, but the indirect allowed bang-gap (E_g) value is the same for both samples, about 3.2–3.3 eV. This is the typical value for a highly disordered WO_3 material [2]. The 60 and 100 °C annealed WO_3 samples gave the same optical spectra (not showed here) as that of the as-deposited WO_3 sample.

XRD patterns (Fig. 2) of the WO_3 films also confirm the lack of long-range order in these samples. The as-deposited WO_3 thin films exhibit a broad diffraction peak at $2\theta \sim 26°$, whereas the 60 and 100 °C annealed ones show an additional broad peak at 2θ around 11–13°. According to literature [17, 24], both peaks are characteristic of the nanocrystalline nature of WO_3 films prepared by electrochemical deposition. But the appearance of the second peak (11–13°) only in annealed samples, together with the positive shift of the peak position as a function of the annealing temperature, leads to the suggestion that it is related to some short-range order. AFM images of the same samples (Fig. 3) also show some effect of the low-temperature annealing on WO_3 samples' morphology. It is observed that the average cluster size in as-deposited WO_3 is between 30 and 40 nm, but it diminishes to 10 nm approximately in annealed samples. The roughness (Rms) values of these samples were: 3.3 nm for as-deposited

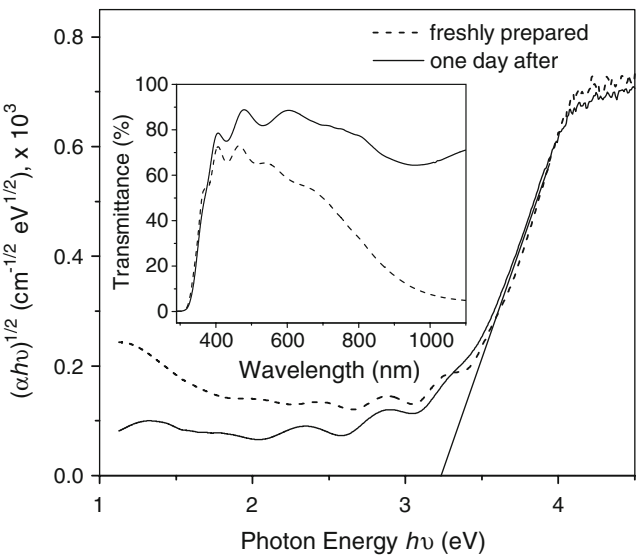

Fig. 1 Optical absorbance and transmittance (*inset*) spectra of freshly prepared and 1-day-after (as-deposited) WO_3 thin films on ITO substrate

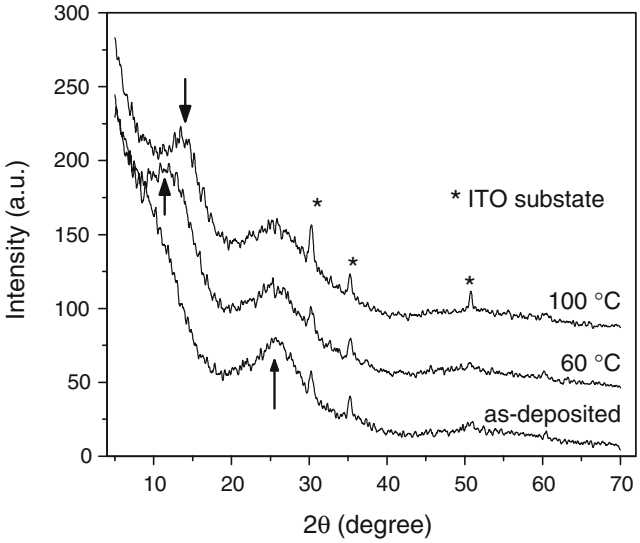

Fig. 2 Low incident angle (5°) XRD spectra of as-deposited, 60 °C, and 100 °C annealed WO_3 films on ITO substrates

films, 3.9 nm for 60 °C and 2.8 nm for 100 °C annealed samples. It means that, after annealing at 60 °C, the roughness of the WO_3 film reaches its maximum; further annealing would reduce the roughness and also the active superficial area of the WO_3 films. Actually, the 100 °C annealed films show a more compact or denser structure (Fig. 3c) and maybe a less porous one compared with the as-deposited and 60 °C annealed samples.

Electrochemical and electrochromic properties of liquid-electrolyte-based devices

Figure 4 shows cyclic voltammograms of the WO_3-based devices assembled with the liquid electrolyte (ITO–WO_3–LiI-PC–ITO) at a scan rate of 20 mV s^{-1} and in the applied potential range between −0.7 V and 0.8 V. (More negative voltage only increases the cathodic current of the cell; at −1.5 V, the current density was around −10 mA cm^{-2}.) These voltammograms exhibit clearly the cathodic and anodic current peaks, which are attributed to the lithium intercalation and deintercalation processes in WO_3 films, respectively, as the result of reductive and oxidative processes. The relationship between the oxidation current peak and the square root of the scan rate was linear (not showed here) and will be discussed later on in the case of polymer gel electrolyte. The blue color, originated from the tungsten bronze formation in the reduction process of WO_3 at −0.5 V or more negative potential values, was observed in the three WO_3-based devices. But the annealing history of the WO_3 film influences on the potential position of the oxidation current peak. The most positive position of oxidation potential corresponds to the 100 °C annealed WO_3 sample, followed by the as-deposited one. The 60 °C annealed WO_3

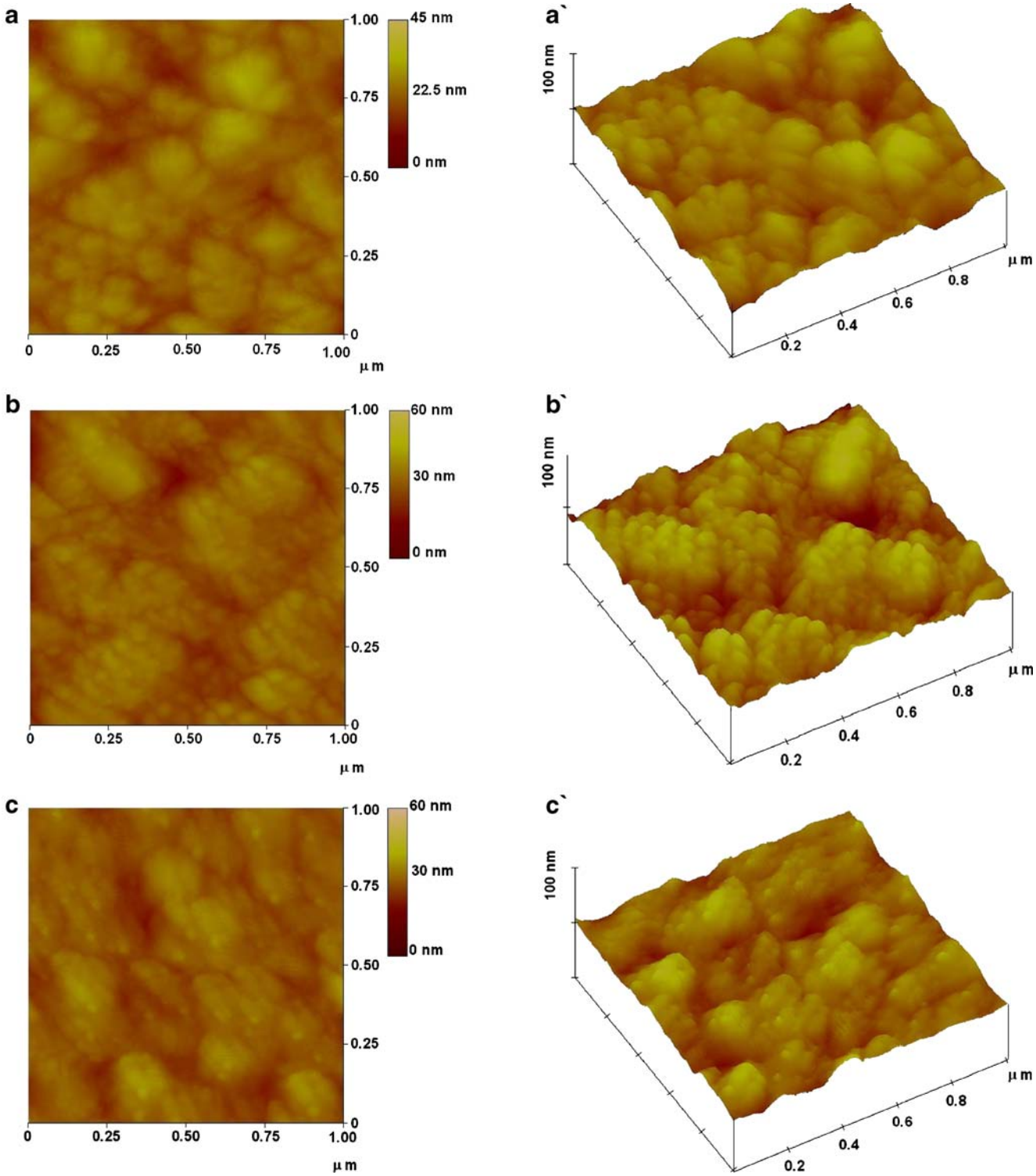

Fig. 3 2-D (*a*, *b*, *c*) and 3-D (*a`*, *b`*, *c`*) AFM images of as-deposited, 60 °C, and 100 °C annealed WO_3 films, respectively

sample gives the most negative oxidative potential. And for reduction case, the order is reversed: the 60 °C annealed sample is the most positive one, followed by the as-deposited sample and the 100 °C annealed sample. From the surface morphology point of view, the 60 °C annealed film (Fig. 3b, b`) shows the highest roughness and the smallest cluster size compared with the as-deposited and 100 °C annealed ones. A higher surface roughness could provide a larger interface

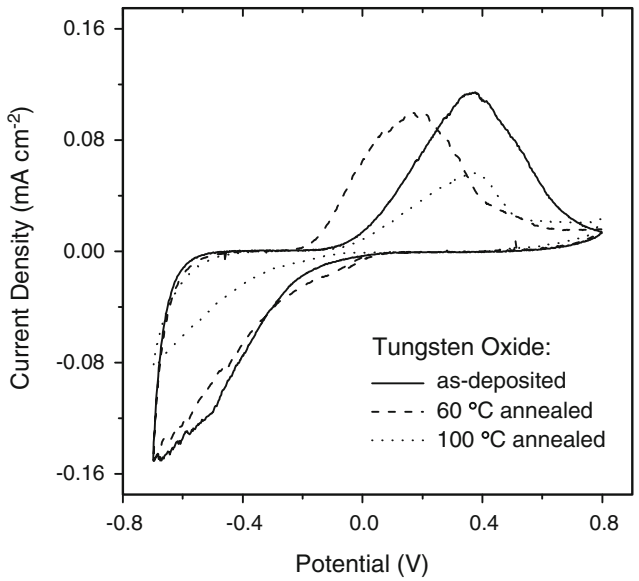

Fig. 4 Cyclic voltammogram curves of as-deposited, 60 °C, and 100 °C annealed WO_3 thin films in sandwiched devices by employing a liquid electrolyte (LiI-PC). The scanning rate was 20 mV s^{-1}

between the WO_3 film and electrolyte and consequently increase the WO_3–Li^+ interaction that helps to reduce the redox potential of the electrochromic film.

The color change due to the electropolarization in WO_3 films is manifested in Fig. 5. For an as-deposited WO_3 sample with the liquid electrolyte, the optical absorbance spectrum of the device at −1.5 V (coloration) is quite different to that at +0.8 V (bleaching). The reduction of WO_3 introduces a new indirect allowed transition with E_g of about 2.6 eV maintaining at the same time the band-gap of the oxidized WO_3 around 3.2 eV. Apparently, the electrochemically reduced WO_3 device shows the same

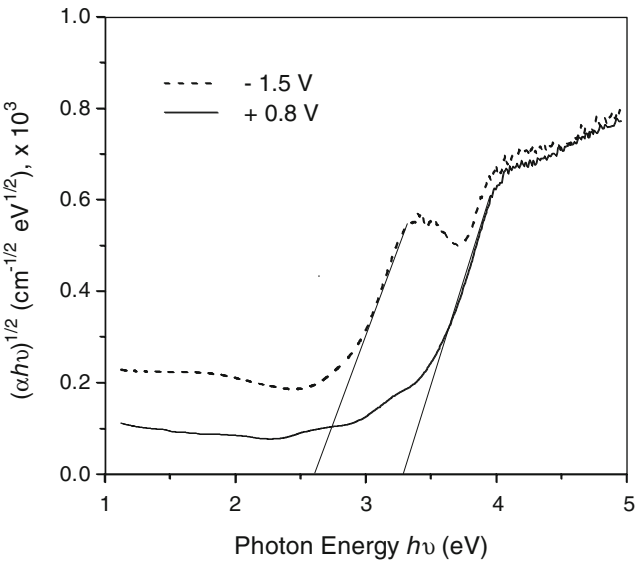

Fig. 5 Optical transmittance spectra of the ITO–(as-deposited)WO_3–LiI-PC–ITO device at −1.5-V and +0.8-V polarization

blue color as the freshly prepared WO_3 film, but they are electronically different. The first is due to the creation of a new band-to-band transition inside the prohibited band of WO_3, and the second one is due to the nonstoichiometry of tungsten oxide, which is unstable in air.

Optical contrast modulations (coloration and bleaching characteristics) at 650 nm of as-deposited and annealed WO_3-film-based devices are illustrated in Fig. 6. The reduction potential was chosen as −1.5 V instead of −1.0 V for the comparison purpose with the polymeric-gel-based devices. It is observed that the optical transmittance change between coloring and bleaching is similar for as-deposited and 60 °C annealed WO_3 films (around 66%). The difference is in the reduction and oxidation speeds: the as-deposited film took longer time to reach the equilibrium values of the optical transmittance at −1.5 V and +1.0 V than the 60 °C annealed WO_3 sample. A possible explanation for this phenomenon could come from the fact that the 60 °C annealed WO_3 films show lower oxidation and reduction potential values (Fig. 4) than those of the as-deposited ones, which helps to increase the switch speeds in optical modulation. For the 100 °C annealed WO_3 samples, it is found that the optical contrast was about 41% in the interval of applied potential, and at the same time lowest switch speeds compared with the other two WO_3 samples. By considering the argument that the higher the redox potential value (Fig. 4) the lower the switching speed, it is reasonable to see a slow optical kinetics in 100 °C annealed WO_3 samples.

It is common to observe that the coloration kinetics (reduction) is slower than the bleaching one (oxidation) for the WO_3 films with liquid electrolyte (Fig. 6). According to

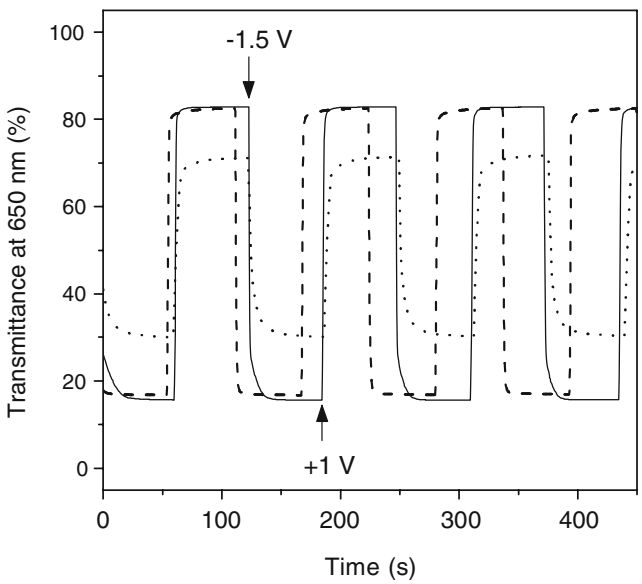

Fig. 6 Optical transmission transient curves of as-deposited (*solid*), 60 °C (*dash*), and 100 °C annealed (*dot*) WO_3 thin films in sandwiched devices by employing a liquid electrolyte (LiI-PC). Switching potentials −1.5 and +1 V

literature [25], this is due to the different mechanisms that govern the two processes: the exchange of current density at the WO_3–electrolyte interface controls the coloration process, whereas the space charge-limited Li^+ ion diffusion current governs the bleaching one. To corroborate this hypothesis, all the transient optical transmittance curves showed in Fig. 6 were fitted by exponential equations, as suggested by our earlier work [26]. It is found that, in most cases, the coloration (reduction) transient curves of WO_3 films with liquid electrolyte can be best fitted by:

$$\Delta T_{\text{coloration}} = A^1_{\text{red}}\left[1 - \exp\left(-t/\tau^{\text{ex1}}_{\text{red}}\right)\right] + A^2_{\text{red}}\left[1 - \exp\left(-t/\tau^{\text{ex2}}_{\text{red}}\right)\right], \quad (1)$$

where the super index *ex* means the charge exchange process, the subindex *red* means reduction, and A is the weight factors of the respective process. At the same time, the bleaching (oxidation) transient curves can be best fitted by:

$$\Delta T_{\text{bleaching}} = A_{\text{ox}}\left[1 - \exp\left(-t/\tau^{\text{dif}}_{\text{ox}}\right)\right], \quad (2)$$

where the subindex ox means oxidation. Parameters τ in Eqs. 1 and 2 are the intervals of time in which the optical transient curves approach to 63% of their equilibrium values. In this way, they are considered as a measurement of the color change rates in each redox process. Table 1 resumes the A (as percentage) and τ (second) values for the three WO_3 devices with the liquid electrolyte. By analyzing the values of $\tau^{\text{dif}}_{\text{ox}}$, it is observed that the as-deposited and 60 °C annealed WO_3 samples show a very similar number for $\tau^{\text{dif}}_{\text{ox}}$ (around 1 s, Table 1), whereas the 100 °C annealed film has a significantly larger value for the same parameter (close to 3 s). If the bleaching process is governed by the space-charge-limited current of charged ionic species and electrons as suggested by literature [2, 25], the lower Li^+ ion diffusion speed (larger $\tau^{\text{dif}}_{\text{ox}}$ value) in the 100 °C annealed WO_3 sample should originate from a higher film density, as commented in the literature [2].

In case of coloration kinetics, the need of two exponential terms for fitting some of the transient curves of WO_3 devices (Table 1) suggests that the surface of tungsten oxide may not be energetically homogeneous for Li^+ ion intercalation; 89% to 100% of the total optical transient curves corresponds to a faster charge transfer speed ($\tau^{\text{ex1}}_{\text{red}}$ varies from 0.43 to 3.13 s) and 11% to 0% to a slower one ($\tau^{\text{ex2}}_{\text{red}}$, from 0 to 18.2 s). For the liquid electrolyte, the 60 °C annealed WO_3 sample showed the most homogenous interfacial potential compared with the as-deposited and 100 °C annealed ones, possibly due to its smaller cluster structure (Fig. 3b, b`). And the 100 °C samples show a slower switching speed (larger value of $\tau^{\text{ex}}_{\text{red}}$) both in oxidation and reduction processes. It seems that the relatively compact surface structure of 100 °C annealed WO_3 samples leads to a higher Li^+ ion intercalation potential energy at the electrolyte–WO_3 interface.

Another useful parameter to describe the electrochromic behavior is the coloration efficiency (η), which is defined as the ratio of the optical density change (ΔOD) to the charge consumed (Q) per unit electrode area (A):

$$\eta = \frac{\Delta \text{OD}}{Q/A}, \text{with } \Delta OD = \log\left(\frac{T_b}{T_c}\right). \quad (3)$$

Here T_b and T_c are the optical transmittance values of the films in the bleached and colored states, respectively. Table 1 also lists the values of the coloration efficiency calculated for the as-deposited and annealed WO_3 films with the liquid electrolyte. The cathodic charge density was determined by step potential techniques, applying a potential of −1.5 V by 20 s. The values of η, from 24.0 to 16.1 $cm^2\ C^{-1}$, were found relatively small in all the three liquid-electrolyte-based WO_3 devices in comparison with the reported values for the same parameter in a three-electrode configuration with a much larger electrolyte volume [17, 27, 28]. The difference may originate from the sandwiched geometry of the devices, which caused a large charge consumption by WO_3 films during the color change, as observed in Fig. 4.

Electrochemical and electrochromic properties of polymer-gel-electrolyte-based devices

Figure 7 corresponds to the electrochemical characterization of the WO_3 devices with polymer gel electrolyte, ITO–WO_3–PMMA-LiI-PC–ITO. The current–voltage curves were recorded at a scan rate of 20 mV s^{-1} in an interval

Table 1 Electrochromic parameters of liquid-electrolyte-based (PC) WO_3 devices

WO_3 films	Coloration time (s)		Bleaching time $\tau^{\text{dif}}_{\text{ox}}$ (s)	T_b (%)	T_c (%)	ΔOD	Cathodic charge (C cm^{-2})	Coloration efficiency ($cm^2\ C^{-1}$)
	$\tau^{\text{ex1}}_{\text{red}}$ (A, %)	$\tau^{\text{ex2}}_{\text{red}}$ (A, %)						
As-deposited	0.43 (92)	5.85 (8)	1.21	82.91	15.63	0.72	0.03	24.0
60 °C	1.01 (100)	0 (0)	0.92	82.39	17.13	0.68	0.29	23.4
100 °C	3.13 (89)	18.21 (11)	2.86	71.34	30.11	0.37	0.023	16.1

Optical transient test wavelength 650 nm, reduction potential −1.5 V, and oxidation potential +1.0 V

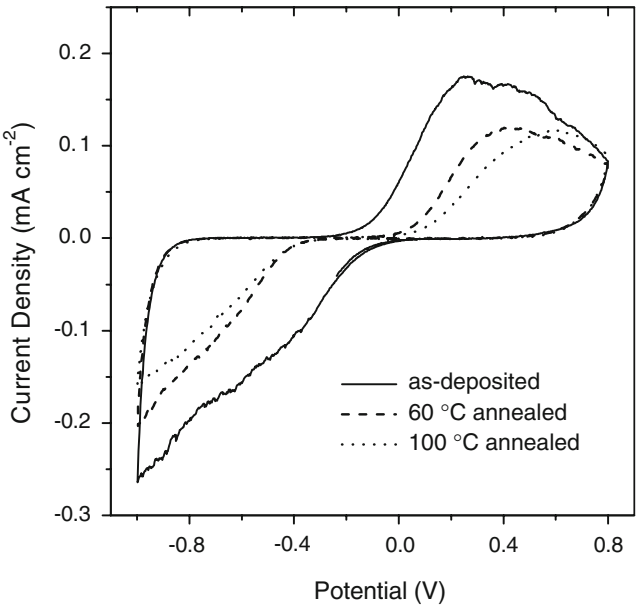

Fig. 7 Cyclic voltammogram curves of as-deposited, 60 °C, and 100 °C annealed WO_3 thin films, respectively, in sandwiched devices by employing a gel electrolyte (PMMA–LiI-PC). The scanning rate was 20 mV s^{-1}

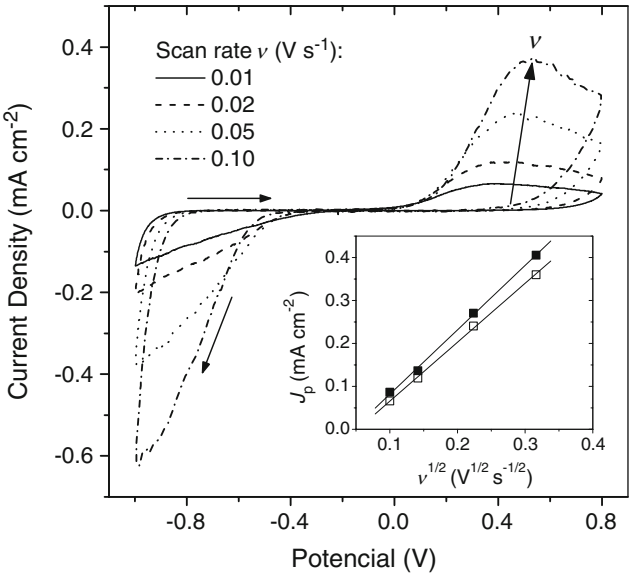

Fig. 8 Cyclic voltammogram curves of 60 °C annealed WO_3 thin film with the PMMA–LiI-PC electrolyte for different scan rate: 10, 20, 50, and 100 mV s^{-1}. *Inset*: Oxidation current peak (J_p, *open square*) and cathodic current at −0.8 V (*filled square*) polarization as a function of the square root of the scan rate (ν)

of −1.0 and 0.8 V. The oxidation peaks in these cases were around 0.3–0.7 V, and the oxidation peak was positively shifted with the annealing temperature. In the case of reduction, the blue color was observed in the devices at more negative potential values (about −0.6 V) compared with the liquid ones (−0.5 V). It means that the presence of PMMA in the electrolyte results in higher redox potentials for the three WO_3 films.

The electrochromism of WO_3 in different electrolytes should be accompanied with the mass transport (Li^+) in the system, which can be probed if the relation between the oxidation current peak (J_p) and the square root of the scan rate (ν) in the cyclic voltammograms of WO_3 devices is linear [29]. Figure 8 only shows the case of 60 °C annealed WO_3 sample with polymer gel electrolyte, in which Levich relation is fulfilled. Actually, for all the WO_3 devices, whether with liquid or polymeric electrolyte, the relation is valid. The difference consists in that the potential of the peak oxidation current is about 0.2 V negatively shifted for liquid-electrolyte-based devices in comparison with the polymeric ones. On the other hand, the reduction peak can never be observed in the mentioned devices, no matter how negative potential is given in CV experiments.

As the optical kinetics concern, it is observed that more than 50% of optical contrasts were observed in all three polymeric-gel-based WO_3 devices (Fig. 9). The coloration efficiency values of these devices (Table 2) are better than those of liquid-electrolyte-based WO_3 devices because of the lower current density observed for coloration. The relatively low optical contrast observed in polymer-gel-based WO_3 electrochromic devices, compared with the liquid electrolyte counterpart, is due to the higher redox potentials required for the polymer system (Fig. 7); the polymer system requires 0.2 V more of applied potential to reach the same optical contrast as the liquid one. Another effect of polymer electrolyte on WO_3 electrochromic performance is the bleaching speed. Table 2 shows that the gel devices give higher values of τ_{ox}^{dif} in comparison

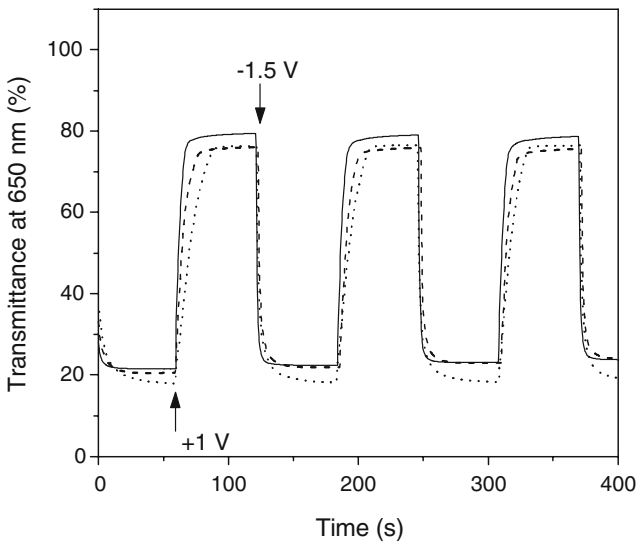

Fig. 9 Optical transmission transient curves of as-deposited (*solid*), 60 °C (*dash*), and 100 °C annealed (*dot*) WO_3 thin films in sandwiched devices by employing a gel electrolyte (PMMA–LiI-PC). Switching potentials −1.5 and +1 V

Table 2 Electrochromic parameters of gel-electrolyte-based (PMMA–LiI-PC) WO_3 devices

WO_3 films	Coloration time (s)		Bleaching time τ_{ox}^{dif} (s)	T_b (%)	T_c (%)	ΔOD	Cathodic charge (C cm^{-2})	Coloration efficiency (cm^2 C^{-1})
	τ_{red}^{ex1} (A, %)	τ_{red}^{ex2} (A, %)						
As-deposited	1.26 (100)	0 (0)	3.40	79.46	21.37	0.57	0.014	40.7
60 °C	1.40 (86)	7.36 (14)	5.34	76.95	21.86	0.54	0.0056	96.4
100 °C	1.80 (56)	11.3 (44)	19.1	76.45	18.36	0.62	0.0075	82.7

Optical transient test wavelength 650 nm, reduction potential −1.5 V, and oxidation potential +1.0 V

with the liquid electrolyte (Table 1) for the three WO_3 samples. It suggests that a lower ionic conductivity in gel electrolyte causes slower space-charge-limited Li^+ ion diffusion inside the electrochromic electrode. Again, the 100 °C annealed WO_3 gives the largest bleaching time due to its relatively compact surface morphology. For coloration kinetic analysis, the polymer-based WO_3 devices show a similar behavior like the liquid ones. The charge exchange process at the electrolyte–electrode interface for as-deposited and 60 °C annealed WO_3 samples is dominated by the fast term, which suggests a lower intercalation potential. The 100 °C annealed WO_3 still exhibit a slow exchange process.

As showed in Tables 1 and 2, the diffusion-controlled optical response times of WO_3 electrochromic devices vary with the annealing temperature of WO_3 samples. Galvanostatic intermittent titration technique was used to determine the chemical diffusion coefficient of Li^+ ions in WO_3. It was proposed by Weppner and Huggins [30], and the technique is based on the injection of Li^+ ions by a known quantity of cathodic charges applied through the electrochemical device. When the charge is interrupted, a new steady stable value (re-equilibration in open circuit) of the potential cell is acquired. The variation of the potential with time and the composition of the intercalation compound are calculated in the plot of potential vs. time, and the diffusion coefficient D can be calculated by following equation:

$$D = \frac{4d^2}{\pi\tau}\left(\frac{\Delta E_s}{\Delta E_t}\right)^2, \quad (4)$$

where ΔE_s represents the change in the steady-state voltages as a result of the current pulse; ΔE_t is the total change in overvoltage during the pulse, thereby eliminating the IR drop, d is the thickness of WO_3 films, and τ is the duration of current pulse. The values of the Li^+ diffusion coefficient were determined in this work for polymeric-gel-electrolyte-based WO_3 devices: 1.98×10^{-10} cm^2 s^{-1} for as-deposited WO_3, 8.49×10^{-11} cm^2 s^{-1} for 60 °C annealed WO_3, and 4.76×10^{-11} cm^2 s^{-1} for 100 °C annealed WO_3 samples. It seems that the more porous the WO_3 films, the larger the chemical diffusion coefficient in WO_3 films, which agrees qualitatively with the τ_{ox}^{dif} values showed in Table 2. The numbers of the diffusion coefficient measured in this work were also close to the reported ones in literature [10, 12, 31, 32].

The long-term stability of the WO_3 films in their electrochromic devices is a major concern in research works, for there are several methods to deposit tungsten oxide thin films. Figure 10 shows the first and the 100th cycles of CV curves of as-deposited and 60 °C annealed WO_3-based devices with polymer electrolyte. The as-deposited WO_3 device loses about 25% of its electrochemical capacity after 100 cycles, and the 60 °C annealed WO_3 one shows a contrary tendency. It suggests that the humidity in WO_3 samples accelerates the switch speed in optical modulation curves (Fig. 9 and Table 2) but deteriorates the long-term stability of the devices. The 100 °C annealed WO_3 sample showed a similar stability as the 60 °C one (not exhibited here). It is encouraging to see that a low-

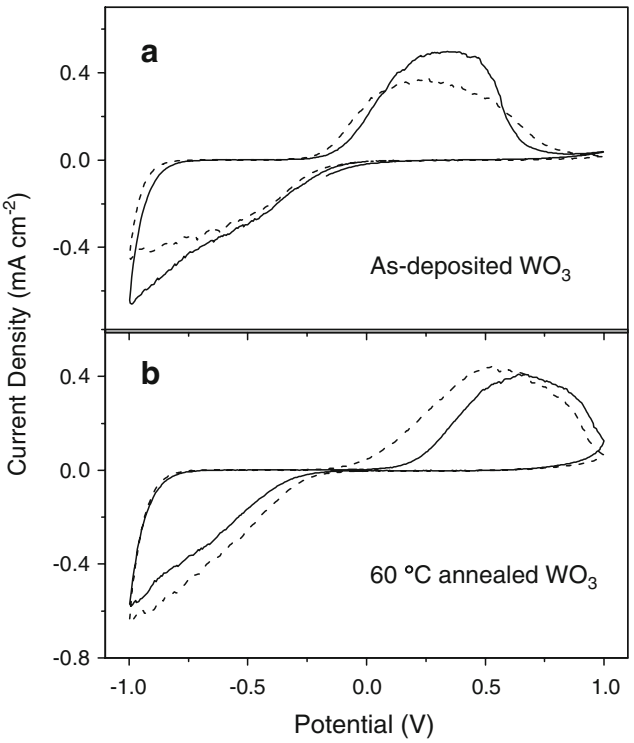

Fig. 10 First and 100th cyclic voltammograms of (*a*) as-deposited (*solid*) and (*b*) 60 °C annealed (*dash*) WO_3-film-based devices with the polymeric gel electrolyte

temperature annealing on WO_3 benefits the stability of its device based on polymeric gel electrolyte.

Conclusions

Electrochemically deposited WO_3 thin films on ITO glass substrates showed different surface morphology as a result of a low-temperature annealing. For as-deposited WO_3 film samples, the surface morphology was porous with a roughness of 3.3 nm, which was increased up to 3.9 nm for 60 °C annealed WO_3 films. In the case of the 100 °C annealed WO_3 samples, the roughness went down to 2.8 nm, and the films showed a more compact structure. The optical response times of the WO_3 devices in coloration (reduction) at −1.5 V and bleaching (oxidation) at +1.0 V varied with the surface morphology of WO_3 films as well as the type of the electrolytes. The reduction process was controlled by the exchange of current density occurring at the interface electrolyte–WO_3; a more porous and rougher WO_3 surface gives a higher ion exchange rate. In the case of oxidation process, the lithium ion diffusion in WO_3 films was the governing process; a larger ionic conductivity of Li^+ in electrolyte and a more porous surface of the WO_3 film accelerate the lithium ion diffusion process in WO_3 films. The effective coloration time in the WO_3 devices varied from 1 to 18 s and the bleaching one from 1 to 19 s.

Acknowledgements The authors thank Rogelio Morán for mechanical design of experimental setup, José Campos for electrical measurement assistance, Ma. Luisa Ramón for XRD experiments, and Mary Cruz Resendiz for AFM images. The financial support from *Programa de Apoyo a Proyectos de Investigación e Inovación Tecnológica de la Universidad Nacional Autónoma de México* (PAPIIT-UNAM, IN104607) and *Consejo Nacional de Ciencia y Tecnología* (CONACyT-México, 42794) is acknowledged.

References

1. Granqvist CG (2000) Solar Energy Materials & Solar Cells 60:201
2. Bange K (1999) Solar Energy Materials & Solar Cells 58:01
3. Sharma N, Deepa M, Varshney P, Agnihotry SA (2000) J Sol-Gel Sci Technol 18:167
4. Avellaneda CO, Bulhões LOS (2003) Solid State Ionics 165:59
5. Biswas PK, Pramanik NC, Mahapatra MK, Ganguli D, Livage J (2003) Materials Letters 57:4429
6. Bueno PR, Faria RC, Avellaneda CO, Leite ER, Bulhões LOS (2003) Solid State Ionics 158:415
7. Kudo T (1984) Nature 312:537
8. Gavanier B, Butt NS, Hutchins M, Mercier V, Topping AJ, Owen JR (1999) Electrochim Acta 44:3251
9. Di Marco G, Lanza M, Pennisi A, Simona F (2000) Solid State Ionics 127:23
10. Mattsson MS (2000) Solid State Ionics 131:261
11. Passerini S, Scrosati B, Hermann V, Holmblad CA, Bartlett T (1994) J Electrochem Soc 141:1025
12. Zhang JG, Tracy CE, Benson DK, Deb SK (1993) J Mater Res 8:2649
13. Yamanaka K (1987) Jpn J Appl Phys 26:1884
14. Meulenkamp E (1997) J Electrochem Soc 144:1664
15. Stevenson KJ, Hurtt GJ, Hupp JT (1999) Electrochem Solid State Lett 2:175
16. Krasnov YS, Kolbasov GY (2004) Electrochem Acta 49:2425
17. Deepa M, Kar M, Agnihotry SA (2004) Thin Solid Films 468:32
18. Gregg BA (1997) Endeavour 21:52
19. Li F, Cheng F, Shi J, Cai F, Liang M, Chen J (2007) Journal of Power Sources 165:911
20. De Paoli MA, Nogueira AF, Machado DA, Longo C (2001) Electrochim Acta 46:4243
21. Li M, Feng S, Fang S, Xiao X, Li X, Zhou X, Lin Y (2007) Electrochim Acta 52:4858
22. Biancardo M, West K, Krebs C (2007) Journal of Photochemistry and Photobiology A: Chemistry 187:395
23. Nogueira AF, De Paoli MA, Montanari I, Monkhouse R, Nelson J, Durrant JR (2001) J Phys Chem B 105:7517
24. Habazaki H, Hayashi Y, Konno H (2002) Electrochim Acta 47:4181
25. Faughnan BW, Crandall RS, Heyman PM (1975) RCA Rev 36:177
26. Hu H, Hechavarría L, Campos J (2003) Solid State Ionics 161:165
27. Srivastava AK, Deepa M, Singh S, Kishore R, Agnihotry SA (2005) Solid State Ionics 176:1161
28. Bessiere A, Badot JC, Certiat MC, Livage J, Lucas V, Baffier N (2001) Electrochim Acta 46:2251
29. Omanovic S, Metikos-Hukovic M (2004) Thin Solid Films 458:52
30. Weppner W, Huggins RA (1977) J Electrochem Soc 124:1569
31. Ho C, Raistrick ID, Huggins RA (1980) J Electrochem Soc 127:343
32. Vijaylakshmi R, Jayachandran M, Sanjeeviraja S (2003) Curr Appl Phys 3:171